Rapid removal of cadmium ions using green-synthesized Fe₃O₄ nanoparticles capped with diethyl-4-(4 amino-5-mercapto-4*H*-1,2,4-triazol-3-yl)phenyl phosphonate†

Sada Venkateswarlu and Minyoung Yoon*

Water-dispersible diethyl-4-(4-amino-5-mercapto-4*H*-triazol-3-yl)phenyl phosphonate (DEAMTPP)-capped biogenic Fe₃O₄ magnetic nanocomposites (DEAMTPP@Fe₃O₄ MNP) have been successfully synthesized using *Ananas comosus* peel pulp extract. The size, structure, magnetic properties, and porosity of the prepared DEAMTPP@Fe₃O₄ MNPs were investigated. The concentration- and pH-dependence of Cd(II)-adsorption properties of the DEAMTPP@Fe₃O₄ MNPs was demonstrated: the adsorption efficiency maximized (96.1%) at pH 6 and at 60 mg L^{-1} of Cd(II) concentration. The maximum Cd(II) adsorption capacity of the DEAMTPP@Fe₃O₄ MNPs, calculated using a Langmuir isotherm, was 49.1 mg g^{-1}, amongst the highest values reported for Cd(II) adsorbents. The ferromagnetic nature of the composite material allows its facile recycling without significant loss of removal efficiency. The excellent adsorption capacity of the nano-adsorbent, together with other advantages like reusability, easy separation, and environmentally-friendly composition, makes it a suitable adsorbent for removal of Cd(II) ions from environmental and industrial wastes.

1. Introduction

Bioaccumulation of heavy metal ions in living cells can adversely affect organ functions in both humans and animals. The major sources of non-biodegradable and untreated heavy metal pollutants (cadmium, arsenic, nickel, chromium, mercury, and lead) in aquatic systems are the rapidly developing industries like electroplating, dyeing, battery manufacturing, mining operations, pharmaceutical industries, tanneries, and glass manufacturing.[1–3] The Cd(II) ion is one of the more hazardous of various heavy metal species, affecting the kidneys, lungs, liver, and reproductive organs in humans, leading to a number of health conditions such as itai-itai disease, renal damage, and emphysema;[4–6] the kidneys are especially vulnerable to Cd(II) toxicity.[7] According to the World Health Organization (WHO) guidelines, the allowable limit of Cd(II) in drinking water is 3 µg L^{-1},[8] and Cd(II) is included on the "red list" of priority substances of the US Environmental Protection Agency.[9] Therefore, the removal of Cd(II) ions from wastewater is a very important issue in water purification. Various technologies, such as chemical precipitation,[10] electrochemical methods (sensors),[11–13] colorimetric method,[14]

membrane filtration,[15] precipitate flotation,[16] biological treatments,[17] coagulation,[18] and adsorption,[19,20] have been proposed to counter heavy metal contamination.

Among the available technologies, adsorption processes have attracted considerable attention because of their effectiveness, availability of materials, low operating cost, flexibility, and simplicity in design and operation.[21] Since the performance of an adsorptive separation technique is directly dependent on the quality and effectiveness of the adsorbent, various noble adsorbents (zeolites,[22] activated carbon,[23] chitosan,[24] clay minerals,[25] tea waste,[26] lignocellulose,[27] and functionalized polymers[28]) have been developed for commercial applications. Nevertheless, most of these adsorbents are either ineffective—due either to diffusion limitation or to insufficient active surface sites—or difficult to separate from wastewater, which make them expensive. Recently, nanoparticles have been considered to provide cost-effective and high-performance Cd(II) removal in water treatment systems. Owing to their large surface area and varied functionalizability, nanoparticles have a greater number of active sites, allowing efficient removal of Cd(II) ions.[29–31] However, practical difficulties in separation processes (*e.g.*, gravitational sedimentation, centrifugation, or filtration) involving common nanoparticles have limited their widespread application.[32]

Magnetic nano-composites have been widely used in various applications including wastewater treatment,[33,34] biomedical drug delivery,[35] magnetic resonance imaging,[36] ferro-fluids

Department of Nanochemistry, College of Bionano, Gachon University, Sungnam, 461-701, Republic of Korea. E-mail: myyoon@gachon.ac.kr

technology,[37] catalysis,[38] and lithium ion batteries,[39] owing to their interesting magnetic behavior. Hence, magnetic adsorbents like porous Fe_3O_4 have been considered ideal water treatment materials to remove heavy metals because of their low operating cost, facile magnetic separation, high adsorption capacities, and thermal stabilities.[40,41] Although many strategies have been developed for the synthesis of magnetic nanoparticles (MNPs) like Fe_3O_4,[42–44] most of the reported processes require the use of organic solvents and reducing agents, which can increase the price of the products and can cause secondary pollution of the environment. To overcome such limitations, the development of environmentally benign and cheap synthetic methods remains a challenging issue. However, only a few green synthetic methods have been reported for Fe_3O_4 synthesis.[45,46] Herein, we present a green synthesis of Fe_3O_4 using *Ananas comosus* (pineapple) peel and further functionalization of the Fe_3O_4 surface with diethyl-4-(4-amino-5-mercapto-4H-1,2,4-triazol-3-yl)phenyl phosphonate (DEAMTPP) as a facile adsorbent for Cd(II) removal from waste water. DEAMTPP is expected to show good Cd(II) removal efficiency because of strong interaction between the thiol functional group on DEAMTPP and Cd(II). To the best of our knowledge, this is the first report of the biogenic synthesis and application of DEAMTPP@Fe_3O_4 MNPs for the removal of Cd(II) from water. The influences of various experimental parameters such as solution pH, initial concentration, and contact time on the adsorption efficiency of DEAMTPP@Fe_3O_4 MNPs were also investigated.

2. Experimental section

2.1 Materials

Ferric chloride hexahydrate ($FeCl_3 \cdot 6H_2O$), sodium acetate ($C_2H_3NaO_2$), HCl, NaOH, DEAMTPP and cadmium nitrate tetrahydrate ($Cd(NO_3)_2 \cdot 4H_2O$) were purchased from Sigma Aldrich, Alfa Aesar, and TCI, and used without further purification. *Ananas comosus* (pineapple) peel pulp was collected from a local market in Sujeong-gu, Sungnam, Gyeonggi-do, South Korea. Deionized Millipore water was used to prepare all solutions.

2.2 Extraction of pineapple (*Ananas comosus*) peel pulp

The Fe_3O_4 MNPs can be prepared by a green-inspired method using waste *Ananas comosus* peel pulp extract to reduce Fe(III) ions because it contains bioactive compounds including sugars (fructose, sucrose, and glucose), esters, polyphenols, and flavonoids,[47,48] which also cap the newly formed Fe_3O_4 MNP surface during their growth processes.[49] The collected pineapple peel pulp was washed with deionized water to remove dust particles and was shade dried at room temperature for about 14 days under dust free conditions. The dried peel pulp (15 g) was blended with water (100 mL) in a 250 mL round-bottom flask and refluxed for 1 h at 70 °C until the color of the aqueous solution changed from clear to yellow. The resulting mixture was cooled to room temperature and was filtered

with cheesecloth. The filtrate was stored at −4 °C in a refrigerator for further experiments.

2.3 Synthesis of DEAMTPP@Fe_3O_4 MNPs

The Fe_3O_4 MNPs were synthesized by a green precipitation method without addition of a chemical reducing agent. In a typical reaction procedure, $FeCl_3 \cdot 6H_2O$ (1.08 g, 4.0 mol) and sodium acetate (3.28 g, 40 mol) are dissolved in freshly prepared pineapple peel pulp extract solution (40 mL) followed by vigorous stirring for 2 h at 80 °C in a 100 mL round bottom flask. After 2 h, the solution attained a homogenous black color. Sodium acetate acts as an electrostatic stabilizing agent for the formation of Fe_3O_4, while the extract solution acts as the reducing agent. The black product obtained was isolated using an external magnetic field and was washed three times with ethanol and water, and then dried in a vacuum oven at 95 °C overnight. The procedure for DEAMTPP synthesis is summarized in Scheme 1. For capping of DEAMTPP on the surface of Fe_3O_4 MNPs, dried Fe_3O_4 MNPs (578 mg) and DEAMTPP (67 mg) were dispersed in ethanol (25 mL) in a 100 mL round-bottom flask and sonicated for 10 h at room temperature (the pH of the reaction mixture was adjusted to 9 by adding 0.1 M NaOH solution). The DEAMTPP-functionalized Fe_3O_4 MNPs were separated by applying an external magnetic field, washed thoroughly thrice with ethanol and deionized water, and finally dried at 95 °C under dynamic vacuum to yield the DEAMTPP@Fe_3O_4 MNPs.

2.4 Characterization

The crystalline structure of DEAMTPP@Fe_3O_4 MNPs was analyzed by powder X-ray diffraction (PXRD) using a Rigaku Ultima III system equipped with a Cu sealed tube ($\lambda = 1.54178$ Å). The following conditions were used: 40 kV, 30 mA, increment = 0.05°, scan speed = 3° min^{-1}. The size and morphology of the as-synthesized particles were determined from images recorded on a Tecnai G^2 transmission electron microscope (TEM), using an accelerating voltage of 300 kV. The compositions of the resulting product were tested by energy dispersive spectroscopy (EDS) with an EDAX analyzer (DPP-II). The magnetization and hysteresis loop were measured at room temperature with a vibrating sample magnetometer (VSM, LKSM-7410). Fourier transform-infrared (FT-IR) spectra of the *Ananas comosus* peel pulp extract and the synthesized samples
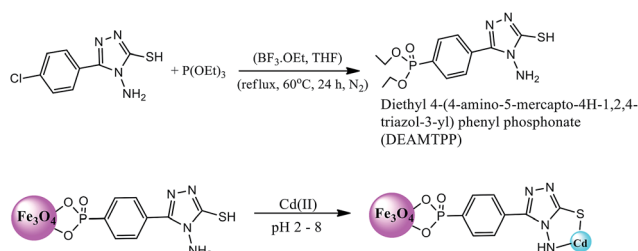
Scheme 1 The procedure for synthesis of DEAMTPP and Fe_3O_4 MNPs functionalized with DEAMTPP.

were recorded on a JASCO FTIR-4600. The iron oxide phase was determined using a LABRAM HR 800 micro Raman spectrometer. For determining the phosphate group conformation, a ^{31}P nuclear magnetic resonance (NMR) Bruker-400 MHZ instrument was used with DMSO-d6 as the solvent and 85% H_3PO_4 as the standard (external solvent). The specific surface area and pore diameter of the nanoparticles were analyzed using a Micromeritics ASAP-2020. High-purity gases (99.999%) were used for the measurements. Thermal gravimetric analysis (TGA) was carried out using on a Linseis L81-I TG-DTA instrument with a heating rate of 10 °C min^{-1} under an N_2 atmosphere.

2.5 Batch adsorption studies

The adsorption studies of Cd(II) ions on DEAMTPP@Fe$_3$O$_4$ MNPs was performed at room temperature. The stock solutions of Cd(II) ions were prepared by dissolving an appropriate quantity of Cd(NO$_3$)$_2$·4H$_2$O in Millipore water to obtain different concentrations, ranging from 20 to 60 mg L^{-1}, with pH varied between 2 and 8. In general, 5 mg of magnetic nano-adsorbent was added to 50 mL of each Cd(II) ion solution. The solution mixture was ultrasonicated for 10 min, transferred to a 100 mL Erlenmeyer flask, and was shaken in an incubator at 25 °C. After each adsorption experiment was performed, the magnetic nano-adsorbent was separated magnetically from the solution. The concentration of Cd(II) ions was determined using atomic absorption spectroscopy (AAS, Shimadzu AA-6300). Each adsorption experiment was repeated thrice. The amount of adsorbed Cd(II) on the magnetic nano-adsorbent in the equilibrium state was calculated using the following equation:

$$q_e = \frac{(C_i - C_e)V}{M} \tag{1}$$

where q_e (mg g^{-1}) is the equilibrium adsorption capacity of Cd(II), C_i and C_e are the initial and equilibrium concentrations (mg L^{-1}), respectively, of Cd(II), and M is the adsorbent dosage (mg). Furthermore, the adsorption percentage was defined as follows:

$$\text{Adsorption (\%)} = \frac{(C_i - C_e)}{C_i} \times 100 \tag{2}$$

The adsorption kinetics using the magnetic nano-adsorbent was studied using an initial Cd(II) concentration of 60 mg L^{-1} at pH 6.0 and an adsorbent dose of 0.5 g L^{-1}.

3. Results and discussions

3.1 Characterization of DEAMTPP@Fe$_3$O$_4$ MNP composite

The phase purity and composition of the prepared materials were characterized by PXRD and FT-IR, ^{31}P NMR, and Raman spectroscopies. The PXRD pattern of DEAMTPP@Fe$_3$O$_4$ MNPs shows diffraction peaks at $2\theta = 18.29°$, 30.08°, 35.43°, 43.07°, 56.98°, 62.54°, and 89.63° (Fig. 1), which is well indexed with the cubic inverse spinel structure of magnetite (Fe$_3$O$_4$) (JCPDS Card no. 74-0748). No diffraction peaks for other iron oxide phases were observed in the PXRD pattern, demonstrating the phase purity of the composite material. In addition, the weak

diffraction intensity and peak broadening may indicate the formation of nano-sized particles. The mean particle size of the resulting composite, determined by the Scherrer equation, was 12 nm. Therefore, the PXRD pattern indicates that the Fe$_3$O$_4$ nanoparticles were successfully synthesized using a green method. In addition, the DEAMTPP anchoring on the surface of Fe$_3$O$_4$ nanoparticles does not induce any phase change in the Fe$_3$O$_4$ MNPs structure.

FT-IR spectra provided direct evidence for the formation of Fe$_3$O$_4$ and for the presence of organic ligands on the surface of MNPs. The presence of aldehydes, amides, and polyphenols in the pineapple peel pulp extract is clearly shown in Fig. 2a. In addition, the peak at 587 cm^{-1} in the IR spectrum of Fe$_3$O$_4$ (Fig. 2b) can be attributed to Fe–O deformation in octahedral and tetrahedral sites.[49] The IR spectra of DEAMTPP (Fig. 2c) and DEAMTPP@Fe$_3$O$_4$ (Fig. 2d) clearly show that DEAMPP is present, covalently bonded to the surface of Fe$_3$O$_4$ MNPs, which can be characterized by an IR peak corresponding to P–O group shift from 1038 to 1014 cm^{-1}.[50,51] In addition, ^{31}P NMR spectra (Fig. S1†) show the successful functionalization of the phosphonate groups on the organic ligand by the substitution reaction (Scheme 1). The peak at 22.4 ppm was attributed to the presence of aromatic phosphate groups on the ligand.

Formation of Fe$_3$O$_4$ MNPs and attachment of DEAMTPP to the MNPs were characterized by Raman spectroscopy for both bare Fe$_3$O$_4$ and DEAMTPP@Fe$_3$O$_4$. For bare Fe$_3$O$_4$ prepared by the green synthesis method, a series of characteristic peaks appeared at 335, 527, 692, and 1384 cm^{-1} corresponding to the Fe–O symmetrical bend and the Fe–O–Fe symmetrical and asymmetrical stretches of Fe$_3$O$_4$ (magnetite) (Fig. 3a).[52] No other characteristic iron oxide peaks, such as those for hematite (α-Fe$_2$O$_3$) and maghemite (γ-Fe$_2$O$_3$), were observed, confirming the phase purity of the green-synthesized Fe$_3$O$_4$ MNPs. After attachment of DEAMTPP to the surface of Fe$_3$O$_4$, no significant change was observed for the peaks corresponding to the Fe$_3$O$_4$ MNP. However, the appearance of the new peaks at 1172, 968, and 476 cm^{-1} (marked by stars) corresponding to the stretching vibrations of DEAMTPP, proves that capping of the Fe$_3$O$_4$ surface by DEAMTPP has occurred (Fig. 3b).[53]

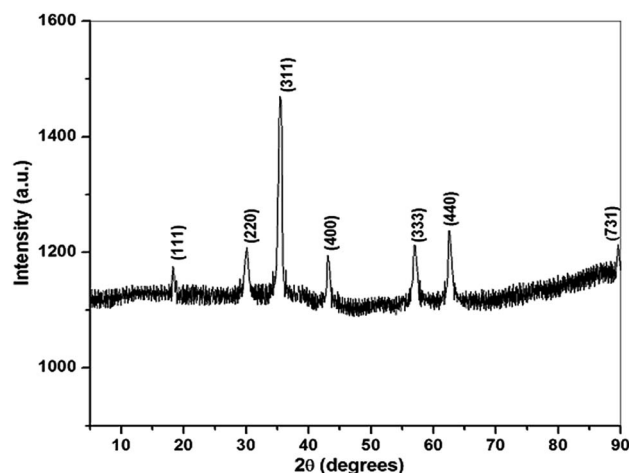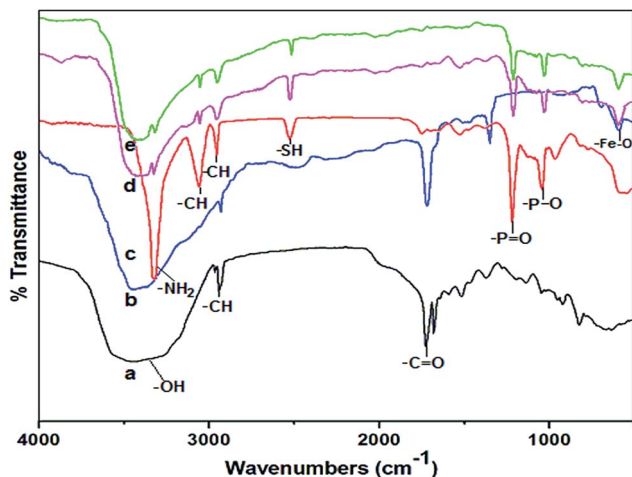Fig. 1 PXRD pattern of DEAMTPP@Fe$_3$O$_4$ MNPs.

Fig. 2 FT-IR spectra of (a) pineapple peel pulp extract (black), (b) Fe_3O_4 MNP (blue), (c) DEAMTPP (red), and (d) DEAMTPP@Fe_3O_4 MNPs (pink). (e) Cd(II) adsorbed DEAMTPP@Fe_3O_4 MNPs.

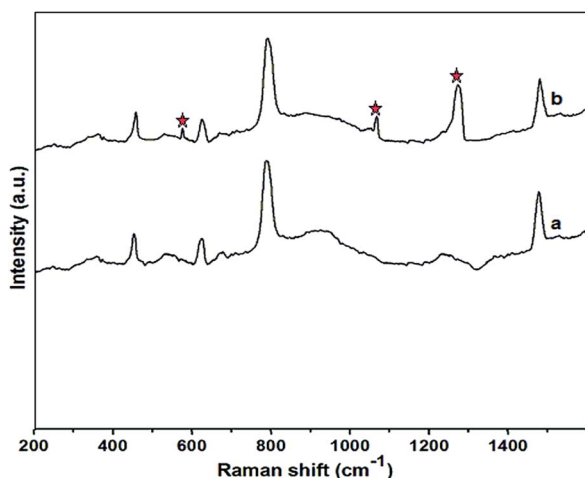**Fig. 3** Raman spectra of (a) Fe_3O_4 MNPs and (b) DEAMTPP@Fe_3O_4 MNPs. Features due to DEAMTPP are marked with stars.

The presence of organic ligands was also proved from the TGA profiles of Fe_3O_4 and DEAMTPP@Fe_3O_4. The TGA profile of Fe_3O_4 MNPs shows a 3.6% weight loss at temperatures below 150 °C due to the desorption of adsorbed water molecules from the MNP mesopores (Fig. 4a). However, DEAMTPP@Fe_3O_4 showed two-step weight loss with the steps commencing at 50 °C and 180 °C. Although the first weight-loss step is similar to that observed for Fe_3O_4, the second step corresponds to the decomposition of organic molecules, confirming the presence of DEAMTPP in the composite material (Fig. 4b). The TGA profile also shows that DEAMTPP@Fe_3O_4 contains 15.7 wt% DEAMTPP (0.58 mmol g^{-1}). In addition, the synthesized composite material is expected to be thermally stable up to 150 °C, but may lose its unique chemical property above this temperature because of the loss of the organic capping ligand (DEAMTPP).
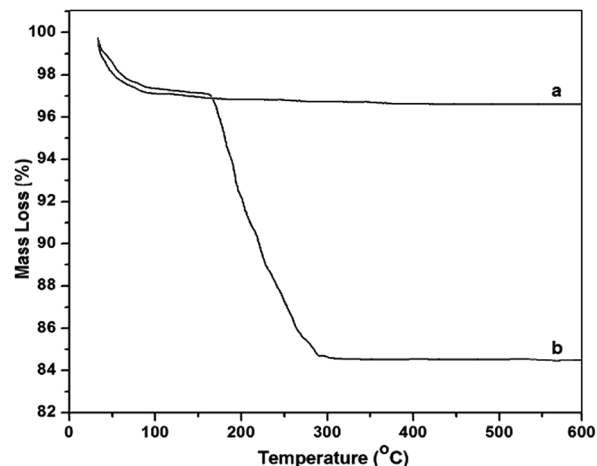
Fig. 4 TGA plots of (a) Fe_3O_4 MNPs and (b) DEAMTPP@Fe_3O_4 MNPs.

The size and morphology of the DEAMTPP@Fe_3O_4 composite nanoparticles were characterized by TEM analysis (Fig. 5). The DEAMTPP@Fe_3O_4 MNPs were nanometer-sized spherical particles with a typical size of approximately 10–16 nm, in good agreement with the size calculated from the PXRD analysis. The MNPs are agglomerated due to the involvement of the hydroxyl groups in the extract, generating mesopores in the composite material. In addition, the corresponding selected area diffraction (SEAD) is shown in the inset of Fig. 5, which displays crystalline diffraction spots of the (111), (220), and (311) planes of the Fe_3O_4 inverse spinal structure. These results match the PXRD data, indicating the nano-crystalline character of the selected area. EDS of DEAMTPP@Fe_3O_4 clearly demonstrates the presence of iron, carbon, oxygen, phosphorus, and sulfur atoms, consistent with the presence of DEAMTPP on the Fe_3O_4 composites (Fig. S2†).

The porosity of the composite material (DEAMPPT@Fe_3O_4) was characterized by N_2 adsorption analysis at 77 K (Fig. 6). The Brunauer–Emmett–Teller (BET) surface area calculated from the N_2 adsorption isotherm was 11.25 m^2 g^{-1}, and the total pore
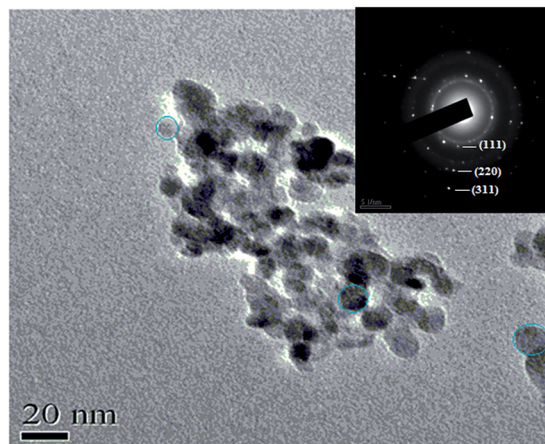

Fig. 5 TEM image and SAED pattern (inset) of DEAMTPP@Fe_3O_4 MNPs.

volume calculated using the single-point adsorption value at $P/P_0 = 0.9972$ was 0.0669 cm^3 g^{-1}. The pore size distribution calculated using the Barrett–Joyner–Halenda (BJH) method shows a uniform mesoporosity of the composite material with a pore size of 13.67 nm (Fig. 6 inset). In addition, the condensation at high values of P/P_0 may suggest the presence of macropores in the composite. The presence of mesopore and macropores in the composite can be useful for the adsorptive removal of heavy metal ions such as Cd(II).

3.2 pH effect on Cd(II) adsorption

The prepared composite material can be used for the removal of heavy metal ions like Cd(II) from water. However, the pH of the metal solution has a strong influence on its chemistry and on the ionic state of the functional groups on the composite surface. Therefore, the effect of pH on the Cd(II) removal efficiency was investigated using Cd(II) stock solutions having pH values in the range 2–8 and various Cd(II) concentrations. The results of this study are summarized in Fig. 7. The Cd(II) removal efficiency using DEAMPPT@Fe$_3$O$_4$ composite increases with increasing pH from 2 to 6, followed by a decrease in efficiency as pH increases beyond 6. At low pH, removal efficiency is low because the high concentration of protons (H$^+$) in solution compete with the Cd(II) ions for the adsorption sites of the adsorbents. Conversely, Cd(II) ions are prone to the formation of Cd(OH)$^+$ and Cd(OH)$_2$,[54] at pH > 6 (aggregation effect between Cd(II) with OH$^-$), lowering the removal efficiency at high pH.[55] In addition, as the Cd(II) concentration increases, the Cd(II) removal efficiency increases and maximizes (96.1%) at 60 mg L^{-1} of Cd(II) concentration at a pH of 6. Therefore, we can conclude that the optimum condition for Cd(II) removal using DEAMPPT@Fe$_3$O$_4$ is pH 6 and 60 mg L^{-1} of Cd(II) concentration.

Finally, the effect of DEAMTPP capping in Cd(II) removal can be analyzed by comparing the Cd(II) removal efficiency of bare Fe$_3$O$_4$ and (with an initial Cd(II) concentration of 60 mg L^{-1}).

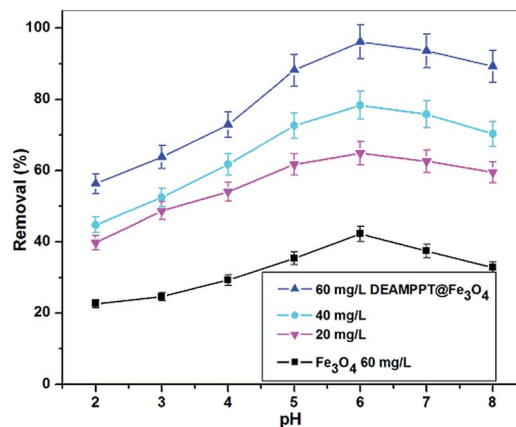**Fig. 6** N$_2$ adsorption/desorption isotherm (at 77 K), and pore size distribution (inset) of the DEAMTPP@Fe$_3$O$_4$ composite.

Fig. 7 Effect of pH on the adsorption of Cd(II) by DEAMTPP@Fe$_3$O$_4$ MNPs at different initial concentrations of Cd(II).

Bare Fe$_3$O$_4$ MNPs showed low Cd(II) removal efficiency (40%) whereas, DEAMTPP@Fe$_3$O$_4$ showed almost complete removal of Cd(II) from the stock solution (96%), suggesting that the DEAMTPP functional group is crucial for the removal of Cd(II). Therefore, we can conclude that a Cd(II) concentration of 60 mL g^{-1} and a pH of 6, with DEAMTPP capping of the Fe$_3$O$_4$ MNP surface, are the optimal conditions for efficient cadmium removal. At these conditions, DEAMTPP@Fe$_3$O$_4$ displays an efficiency of Cd(II) removal from aqueous solution that is among the highest for heavy metal adsorbent materials. The pH effect on Cd(II) adsorption by DEAMTPP@Fe$_3$O$_4$ can be explained by the following mechanism.

Although the organic capping ligand (DEAMTPP) has an important role in removal of Cd(II) ions, the exact mechanism is not clearly understood. For better understanding of the Cd(II) adsorption mechanism, we compared IR spectra of the composite, before (Fig. 2d) and after Cd(II) adsorption (Fig. 2e). The IR peaks at 3332 and 2522 cm^{-1} corresponding to stretching of amine and mercapto group, respectively, before adsorption, were shifted to 3312 and 2508 cm^{-1} after adsorption. IR peak shift to lower wavenumber suggests Cd(II) coordination to the mercapto and the amine functional groups of DEAMTPP. By combining the Cd(II) adsorption experiment and IR analysis, we expect that Cd(II) can be removed by coordination to the capping organic ligand (Scheme 2).

3.3 Effect of adsorbent dosage

The optimal adsorbent dosage in terms of Cd(II) adsorption (equilibrium) capacity of the functionalized MNPs was investigated at pH 6.0 by varying the adsorbent dosage from 0.02 to 0.14 g L^{-1} (Fig. S3†). It is apparent that the Cd(II) removal efficiency drastically increased from 17% to 96% as the doses of DEAMTPP@Fe$_3$O$_4$ MNPs increased from 0.02 to 0.1 g L^{-1}. When the adsorbent dose increases, the sorption of Cd(II) increases, because more active sites on the adsorbent were obviously becoming available.[56] However, it is saturated at 0.1 g L^{-1} dosage without showing further efficiency enhancement of
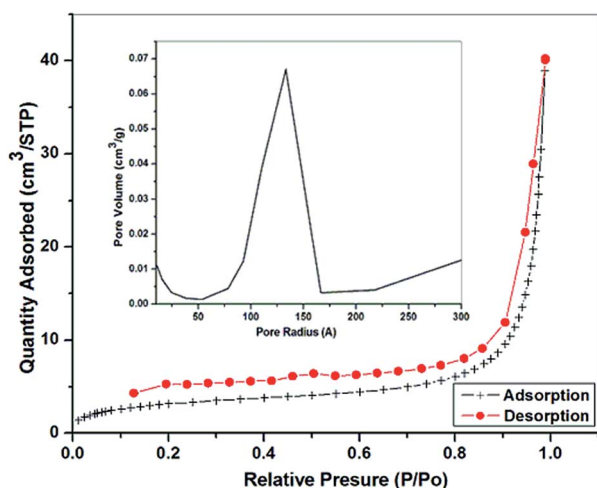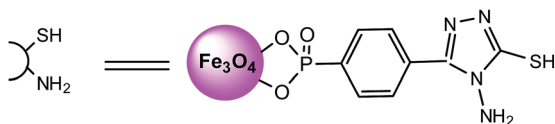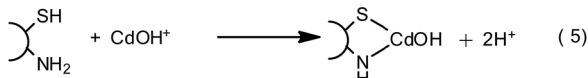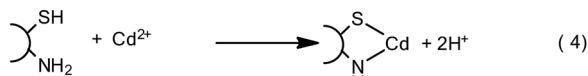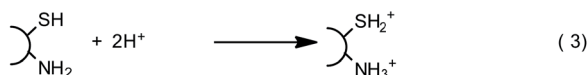
Scheme 2 Proposed mechanism for Cd(II) ion removal.

Cd(II) ion removal on increasing the dosage. Thus, 0.1 g L^{-1} of DEAMTPP@Fe$_3$O$_4$ was used in subsequent experiments.

3.4 Adsorption kinetics of Cd(II)

The effect of contact time on Cd(II) sorption was studied at pH 6.0 for a solution with an initial Cd(II) concentration of 60 mg L^{-1} (Fig. 8). The adsorption proceeds rapidly and an adsorption equilibrium was reached within 60 min. The kinetics of Cd(II) adsorption could not be fit on the magnetic nano-composite with a pseudo-first-order model.[57]

The pseudo-first-order kinetic model is given by the following equation (eqn (3)):

$$\log(q_e - q_t) = \log q_e - \left(\frac{k_1}{2.303}\right)t \qquad (3)$$

where k_1 (min^{-1}) is the pseudo-first-order rate constant of adsorption, and q_e and q_t (mg g^{-1}) are the amounts of Cd(II) adsorbed at equilibrium and at time t, respectively (calculated parameters are presented in ESI†).

A pseudo-second-order kinetic model[58] was also applied to the analysis of the Cd(II) adsorption kinetic data. The linear form of the equation representing this model is as follows (eqn (4)):

$$\frac{t}{q_t} = \frac{1}{k_2 q_e^2} + \left(\frac{1}{q_e}\right)t \qquad (4)$$

where k_2 (g mg^{-1} min^{-1}) is the pseudo-second-order rate constant.

Adsorption data fitted well with the pseudo-second-order kinetic model (Fig. 9), with a correlation coefficient value (R^2) of 0.9955 (parameters for pseudo-second-order kinetics are summarized in Table S1†). Therefore, we can conclude that the kinetics of Cd(II) adsorption on DEAMTPP@Fe$_3$O$_4$ MNPs follow the pseudo-second-order model; this supports the assumption that the form of adsorption is chemisorption.[59]

3.5 Adsorption isotherm analysis

To evaluate the distribution of Cd(II) ions in the liquid/solid interphase at equilibrium during adsorption, the room-temperature adsorption capacities of Cd(II) were calculated at pH 6 using two typical adsorption models. The Langmuir isotherm describes monolayer adsorption of molecules on a solid surface, whereas the Freundlich isotherm describes multilayer adsorption with random distribution. The Langmuir equation can be expressed in a linear form as follows:

$$\frac{C_e}{q_e} = \frac{C_e}{q_m} + \frac{1}{q_m b} \qquad (5)$$

where q_e is the amount of adsorbed metal ions at equilibrium for a metal ion concentration in solution of C_e, q_m is the maximum capacity of the adsorbent, and b is the equilibrium constant related to the sorption energy.

The Langmuir equation provides a good fit to the adsorption data (Fig. 10a), and the calculated maximum adsorption capacity for DEAMTPP@Fe$_3$O$_4$ MNPs was 49.1 mg g^{-1} at pH 6 and an initial concentration of 60 mg L^{-1} (Table S2†). In addition, a separation factor, R_L, calculated using equation (eqn (6)), elucidates the spontaneity of the adsorption process. It is assumed that if $0 < R_L < 1$, the adsorption process is favorable. The calculated R_L value for the adsorption of Cd(II) on
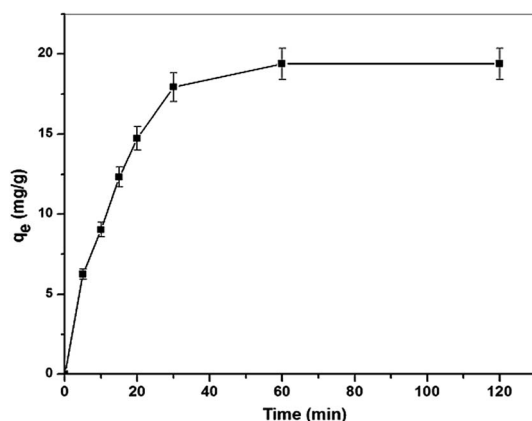

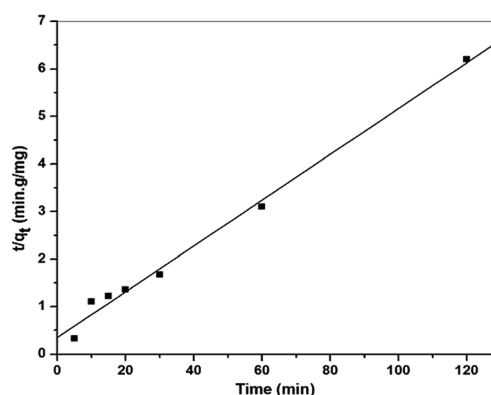**Fig. 8** Time dependence of Cd(II) adsorption capacity on DEAMTPP@Fe$_3$O$_4$ MNPs.

Fig. 9 Pseudo second-order kinetics of Cd(II) adsorption on DEAMTPP@Fe$_3$O$_4$ MNPs.

DEAMTPP@Fe$_3$O$_4$ MNPs was 0.0898, and thus Cd(II) adsorption is favorable.

$$R_L = \frac{1}{1 + bC_i} \quad (6)$$

where C_i is initial metal concentration, and b is the Langmuir constant.

The Freundlich isotherm can be applied to the metal ion adsorption model on a heterogeneous surface, and the linear form of isotherm is expressed as:

$$\log q_e = \log k_f + \frac{1}{n} \log C_e \quad (7)$$

where k_f and n are the Freundlich isotherm constants that represent the adsorption of adsorbents.

The linear Freundlich isotherm provided a good fit to the adsorption data (Fig. 10b), giving a Cd(II) adsorption isotherm of DEAMTPP@Fe$_3$O$_4$ MNPs. Constants calculated from the isotherm data are summarized in Table S2,† and the n value (<1) indicates a favorable adsorption condition.[60,61] Although the Cd(II) adsorption data can be fitted well using both Langmuir and Freundlich models, the Langmuir model gives a more reliable fit, suggesting that Cd(II) adsorption onto the DEAMTPP@Fe$_3$O$_4$ MNPs occurs in a monolayer coverage. This result suggests that surface functionalization using the organic capping ligand is important for enhancement of the capacity and efficiency of Cd(II) adsorption by the MNPs. The adsorption capacity of the present DEAMTPP@Fe$_3$O$_4$ MNPs is compared with that reported for other materials in Table

1.[62–68] It should be noted that the prepared material showed a better Cd(II) adsorption capacity than other organic-molecule-capped MNPs,[66,67] and a value similar to the best adsorption capacity among the reported materials.[68]

3.6 Adsorption selectivity

For investigation of selective adsorption, a mixed solution of metal ions containing Cd(II), Co(II), Zn(II), Cu(II), and Ni(II) were prepared, concentrations of all the heavy metal ions set at ∼60 mg L^{-1}. The adsorption of Cd(II) from the mixed metal ion solution using DEAMTPP@Fe$_3$O$_4$ MNPs shows efficiency similar to the adsorption experiment using pure Cd(II) ion solution. The composite shows much higher removal efficiency for Cd(II) ions than the other metal ions (Fig. S4†) in an order of Cd(II) > Zn(II) > Cu(II) > Co(II) > Ni(II). The Cd(II) ion selectivity is due to the presence of mercapto and amine groups on the surface of the adsorbent and the mercapto group plays a major role in the Cd(II)-selectivity due to softness of the base. According to the Hard–Soft Acid–Base (HSAB) theory,[69] interactions between soft acid and soft base predominate. Cd(II) is a soft acid which can preferably interact with the soft basic mercapto group over other metal ions. As the other metal ions are borderline acids, they interact weakly with mercapto groups. This result clearly demonstrates selective sorption of Cd(II) onto the surface of DEAMTPP@Fe$_3$O$_4$ MNPs without interference from the other metal ions.

3.7 Magnetic separation and recycle study

The magnetic properties of bare Fe$_3$O$_4$ and DEAMTPP@Fe$_3$O$_4$ MNPs were evaluated by examining the magnetic hysteresis loops at room temperature (Fig. 11). The presence of the hysteresis loop demonstrates the ferromagnetic behavior of the bare Fe$_3$O$_4$ and the DEAMTPP@Fe$_3$O$_4$ MNPs. The saturation magnetization (M_s) for the bare Fe$_3$O$_4$ and DEAMTPP@Fe$_3$O$_4$ MNPs were 21.7 and 16.9 emu g^{-1}, respectively. The decrease of saturation magnetization for the functionalized nanoparticles is due to quenching of the magnetic moment by interactions between the coated organic molecules (DEAMTPP) and Fe$_3$O$_4$. The ferromagnetic character is also revealed by the results, which show a nonzero remanent magnetization (M_r) and a coercive force (H_c) in the non-linear hysteresis loop (Fig. 11 inset).[70] Due to the
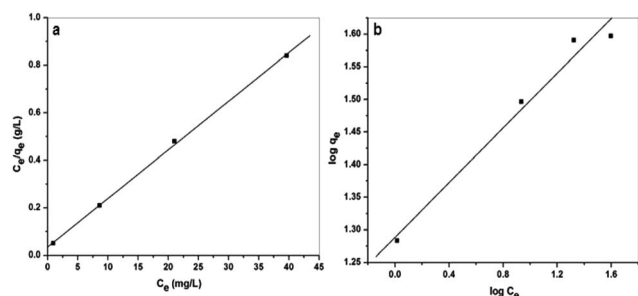

Fig. 10 Fit of data for Cd(II) sorption on DEAMTPP@Fe$_3$O$_4$ MNPs to (a) the Langmuir isotherm, and (b) the Freundlich isotherm.

Table 1 Comparison of adsorption capacities of various adsorbents for Cd(II) removal from water

Type of adsorbent	Adsorption capacity (mg g^{-1})	Reference
Polyaniline grafted chitosan	14.3	62
Coffee grounds	15.6	63
Fe$_3$O$_4$–P(Cys/HEA) hydrogel	19.5	64
Chitosan modified with sulfoxine chelate agent	32.9	65
Fe$_3$O$_4$–cyclodextrin	22.7	66
Fe$_3$O$_4$–GS	27.8	67
Thiocyanato-functionalized silica gel	49.3	68
DEAMTPP@Fe$_3$O$_4$ MNPs	49.1	This work

4 M. P. Mahalik, W. H. Henry and C. P. Walter, *Toxicol. Lett.*, 1995, **76**, 195–202.

5 P. W. Micheal, *J. Inorg. Biochem.*, 2000, **79**, 241–244.

6 S. Benoff, A. Jacob and I. R. Hurley, *Hum. Reprod. Update*, 2000, **6**, 107–121.

7 Y. H. Li, S. Wang, Z. Luan, J. Ding, C. Xu and D. Wu, *Carbon*, 2003, **41**, 1057–1062.

8 WHO, *Guidelines for Drinking-Water Quality*, Recommendations World Health Organization, Geneva, 3rd edn, 2004, vol. 1.

9 US Environmental Protection Agency, *Integrated Risk Information System (IRIS) on Cadmium*, National Center for Environmental Assessment, Office of Research and Development, Washington, DC, 1999.

10 E. G. Segura, M. S. Ríos, A. C. Cruz and C. Fall, *J. Environ. Manage.*, 2012, **97**, 6–13.

11 S. Bayar, A. E. Yilmaz, R. Boncukcuoglu, B. A. Fil and M. M. Kocakerim, *Desalin. Water Treat.*, 2013, **51**, 2635–2643.

12 X. Chai, L. Zhang and Y. Tian, *Anal. Chem.*, 2014, **86**, 10668–10673.

13 G. Liu, Y. Zhang, M. Qia and F. Chen, *Anal. Methods*, 2015, **7**, 5619–5626.

14 Y. Guo, Y. Zhang, H. Shao, Z. Wang, X. Wang and X. Jiang, *Anal. Chem.*, 2014, **86**, 8530–8534.

15 M. Garmsiri and H. R. Mortaheb, *Chem. Eng. J.*, 2015, **264**, 241–250.

16 M. R. Mahmoud, N. K. Lazaridis and K. A. Matis, *Process Saf. Environ. Prot.*, 2015, **94**, 203–211.

17 M. G. S. Martínez, E. L. Silva, R. Encalada, E. Pineda, J. C. G. Pérez, A. Z. Rodriguez, R. M. Sánchez, E. Saavedra and R. J. Chávez, *J. Hazard. Mater.*, 2015, **288**, 104–112.

18 S. Vasudevan, J. Lakshmi and G. Sozhan, *J. Hazard. Mater.*, 2011, **192**, 26–34.

19 I. Ali and V. K. Gupta, *Nat. Protoc.*, 2007, **1**, 2661–2667.

20 P. O. Boamah, Y. Huang, M. Hua, Q. Zhang, Y. Liu, J. Onumah, W. Wang and Y. Song, *Carbohydr. Polym.*, 2015, **122**, 255–264.

21 D. P. Quintanilla, I. d. Hierro, M. Fajardo and I. Sierra, *J. Mater. Chem.*, 2006, **16**, 1757–1764.

22 J. C. Izidoro, D. A. Fungaro, J. E. Abbott and S. Wang, *Fuel*, 2013, **103**, 827–834.

23 T. M. Alslaibi, I. Abustan, M. A. Ahmad and A. A. Foul, *J. Environ. Chem. Eng.*, 2013, **1**, 589–599.

24 L. Huang, S. Yuan, L. Lv, G. Tan, B. Liang and S. O. Pehkonen, *J. Colloid Interface Sci.*, 2013, **405**, 171–182.

25 V. K. Gupta and S. Sharma, *Environ. Sci. Technol.*, 2002, **36**, 3612–3617.

26 S. Wan, Z. Ma, Y. Xue, M. Ma, S. Xu, L. Qian and Q. Zhang, *Ind. Eng. Chem. Res.*, 2014, **53**, 3629–3635.

27 E. W. Shin, K. G. Karthikeyan and M. A. Tshabalala, *Bioresour. Technol.*, 2007, **98**, 588–594.

28 V. Singh, A. K. Sharma and S. Maurya, *Ind. Eng. Chem. Res.*, 2009, **48**, 4688–4696.

29 A. G. Mamalis, *J. Mater. Process. Technol.*, 2007, **181**, 52–58.

30 T. Sangvanich, J. Morry, C. Fox, W. Ngamcherdtrakul, S. Goodyear, D. Castro, G. E. Fryxell, R. S. Addleman, A. O. Summers and W. Yantasee, *ACS Appl. Mater. Interfaces*, 2014, **6**, 5483–5493.

31 S. B. Khan, M. M. Rahman, H. M. Marwani, A. M. Asiri and K. A. Alamry, *Nanoscale Res. Lett.*, 2013, **8**, 377–384.

32 L. X. Wang, J. C. Li, Q. Jiang and L. J. Zhao, *Dalton Trans.*, 2012, 4544–4551.

33 Y. Wang, L. Wang, T. Tian, X. Hu, Q. Xu and C. Yang, *Anal. Methods*, 2013, **5**, 1856–1862.

34 F. Liu, Y. Jin, H. Liao, L. Cai, M. Tong and Y. Hou, *J. Mater. Chem. A*, 2013, **1**, 805–813.

35 S. D. Kong, W. Zhang, J. H. Lee, K. Brammer, R. Lal, M. Karin and S. Jin, *Nano Lett.*, 2010, **10**, 5088–5092.

36 E. S. Shibu, K. Ono, S. Sugino, A. Nishioka, A. Yasuda, Y. Shigeri, S. Wakida, M. Sawada and V. Biju, *ACS Nano*, 2013, **7**, 9851–9859.

37 S. H. Sun, C. B. Murray, D. Weller, L. Folks and A. Moser, *Science*, 2000, **287**, 1989–1992.

38 D. Wang and D. Astruc, *Chem. Rev.*, 2014, **114**, 6949–6985.

39 J. Zhao, B. Yang, Z. Zheng, J. Yang, Z. Yang, P. Zhang, W. Ren and X. Yan, *ACS Appl. Mater. Interfaces*, 2014, **6**, 9890–9896.

40 T. Wang, L. Zhang, H. Wang, W. Yang, Y. Fu, W. Zhou, W. Yu, K. Xiang, Z. Su, S. Dai and L. Chai, *ACS Appl. Mater. Interfaces*, 2013, **5**, 12449–12459.

41 J. Jin, F. Yang, F. Zhang, W. Hu, S. Sun and J. Ma, *Nanoscale*, 2012, **4**, 733–736.

42 Q. Zhang, R. Chen, J. Gong, M. Yuan and L. Chen, *J. Alloys Compd.*, 2013, **577**, 528–532.

43 J. S. Chen, Y. Zhang and X. W. Lou, *ACS Appl. Mater. Interfaces*, 2011, **3**, 3276–3279.

44 S. Laurent, D. Forge, M. Port, A. Roch, C. Robic, L. V. Elst and R. N. Muller, *Chem. Rev.*, 2008, **108**, 2064–2110.

45 A. Demir, R. Topkaya and A. Baykal, *Polyhedron*, 2013, **65**, 282–287.

46 Y. Cai, Y. Shen, A. Xie, S. Li and X. Wang, *J. Magn. Magn. Mater.*, 2010, **322**, 2938–2943.

47 A. P. Bartolome and P. Ruperez, *J. Agric. Food Chem.*, 1995, **43**, 608–612.

48 M. Amzad Hossain and S. M. Mizanur Rahman, *Food Res. Int.*, 2011, **44**, 672–676.

49 S. Venkateswarlu, Y. SubbaRao, T. Balaji, B. Prathima and N. V. V. Jyothi, *Mater. Lett.*, 2013, **100**, 241–244.

50 T. J. Daou, S. B. Colin, J. M. Greneche, F. Thomas, A. Derory, P. Bernhardt, P. Legare and G. Pourroy, *Chem. Mater.*, 2007, **19**, 4494–4505.

51 C. Lu, L. R. Bhatt, H. Y. Jun, S. H. Park and K. Y. Chai, *J. Mater. Chem.*, 2012, **22**, 19806–19811.

52 M. Basu, A. K. Sinha, S. Sarkar, M. Pradhan, S. M. Yusuf, Y. Negishi and T. Pal, *Langmuir*, 2010, **26**, 5836–5842.

53 A. M. Milankovic, A. Santic, S. T. Reis, K. Furic and D. E. Day, *J. Non-Cryst. Solids*, 2004, **342**, 97–109.

54 J. Duan and B. Su, *Chem. Eng. J.*, 2014, **246**, 160–167.

55 G. Yang, L. Tang, X. Lei, G. Zeng, Y. Cai, X. Wei, Y. Zhou, S. Li, Y. Fang and Y. Zhang, *Appl. Surf. Sci.*, 2014, **292**, 710–716.

56 A. Mirabi, Z. Dalirandeh and A. S. Rad, *J. Magn. Magn. Mater.*, 2015, **381**, 138–144.

57 Z. Y. Yao, J. H. Qi and L. H. Wang, *J. Hazard. Mater.*, 2010, **174**, 137–143.

58 Y. S. Ho and G. Mckay, *Process Biochem.*, 1999, **34**, 451–465.

59 G. Crini, H. N. Peindy, F. Gimbert and C. Robert, *Sep. Purif. Technol.*, 2007, **53**, 97–110.

60 B. H. Hameed, D. K. Mahmoud and A. L. Ahmad, *J. Hazard. Mater.*, 2008, **158**, 65–67.

61 J. Gong, T. Liu, X. Wang, X. Hu and L. Zhang, *Environ. Sci. Technol.*, 2011, **45**, 6181–6187.

62 R. Karthik and S. Meenakshi, *Chem. Eng. J.*, 2015, **263**, 168–177.

63 N. Azouaoua, Z. Sadaoui, A. Djaafri and H. Mokaddem, *J. Hazard. Mater.*, 2010, **184**, 126–134.

64 R. Hua and Z. Li, *Chem. Eng. J.*, 2014, **249**, 189–200.

65 L. Vitali, M. C. M. Laranjeira, N. S. Goncalves and V. T. Favere, *Int. J. Biol. Macromol.*, 2008, **42**, 152–157.

66 Z. M. Badruddoza, Z. B. Z. Shawon, W. J. D. Tay, K. Hidajat and M. S. Uddin, *Carbohydr. Polym.*, 2013, **91**, 322–332.

67 X. Guo, B. Du, Q. Wei, J. Yang, L. Hu, L. Yan and W. Xu, *J. Hazard. Mater.*, 2014, **278**, 211–220.

68 Z. Li, H. Fan, Y. Zhang, M. Chen, Z. Yu, X. Cao and T. Sun, *Chem. Eng. J.*, 2011, **171**, 703–710.

69 R. G. Person, *Inorg. Chem.*, 1988, **27**, 734–740.

70 M. Fangzhi, G. Jianguo, M. Huiru, X. Leilei and S. Weidong, *ACS Appl. Mater. Interfaces*, 2012, **4**, 3987–3993.